Banding of angular velocity in the current-driven vortex lattice of a type-II superconductor

Akira Furukawa[1] and Yunori Nisikawa[2]
[1]*Yukawa Institute for Theoretical Physics, Kyoto University, Kyoto 606-8502, Japan*
[2]*Department of Material Science, Osaka City University, Osaka 558-8585, Japan*
(Received 7 October 2005; published 14 February 2006)

We phenomenologically investigate a possible mechanism of the banding of angular velocity in a current-driven vortex lattice in type-II superconductors. It is shown that the plastic motion occurs above some critical value of the applied current, resulting in a splitting in the vortex lattice. The present model can qualitatively reproduce major features of the experimental results reported by Lopez *et al.* [Phys. Rev. Lett. **82**, 1277 (1999)].

DOI: 10.1103/PhysRevB.73.064511 PACS number(s): 74.25.Qt, 62.20.Fe, 46.35.+z

I. INTRODUCTION

In the last two decades vortex matter in type-II superconductors has attracted considerable attention from both fundamental and technological viewpoints. Even in equilibrium we can see various interesting properties of vortex phases. That is, depending on the values of the magnetic field, temperature, and strength of the quenched disorder, the vortices can form liquid, solid, and glassy phases, similar to ordinary condensed matters.[1,2] Because the electric resistivity is one of the most important physical properties of superconductors, understanding current-driven vortices is of great importance and the nonequilibrium dynamics of vortices is a research area which has grown rapidly.

Lopez *et al.* previously reported interesting experimental results of current-driven vortex dynamics in high-T_c superconductors $YBa_2Cu_3O_{7-\delta}$ in a solid phase near the first-order melting temperature.[3,4] The sample geometry used in their experiments is the so-called Corbino disk (Fig. 1), which can provide radially an inhomogeneous driving force. A magnetic field B_0 parallel to the disk axis is applied, and a current I is injected at the center of the disk and is ejected at the outer boundary, which gives rise to an inhomogeneous radial current density

$$J(r) = \frac{I}{2\pi \ell\, r}, \tag{1}$$

where r is the distance from the disk center and ℓ is the thickness of the disk. This radial current density creates the azimuthal Lorentz force

$$\mathbf{f}_L = B_0 J(r)\hat{\phi}, \tag{2}$$

where $\hat{\phi}$ is the unit vector in the azimuthal direction. The Lorentz force $\mathbf{f}_L$ acts as an external driving force on the vortices.

In a solid phase, the dynamics of the displacement field $\mathbf{u}$ of the vortex solids is described by the equation of motion (see Ref. 5 for example)

$$0 = -\gamma \mathbf{v} + \nabla \cdot \vec{\boldsymbol{\sigma}}^{\mathrm{el}} + \mathbf{f}_L, \tag{3}$$

where $\mathbf{v} = \partial \mathbf{u}/\partial \mathbf{t}$ and the first term represents the effective friction force density, so-called Bardeen-Stephen friction force.[6] The second term is the elastic force density due to the interaction among vortices, and the last term is the Lorentz force. Here, we neglect the pinning force arising from impurities, assuming a clean system.

In the experiment,[3,4] for a relatively low applied current, the vortex lattice moves coherently over the whole system, resulting in the velocity profile $\sim r$. It can be well described within the framework of the linear elasticity:

$$\nabla \cdot \vec{\boldsymbol{\sigma}}^{\mathrm{el}} \cong c_{66} \nabla^2 \mathbf{u}, \tag{4}$$

where c_{66} is the shear elastic modulus and we make use of the incompressibility condition $\nabla \cdot \mathbf{u} = \mathbf{0}$ in ordinary systems. We can solve Eq. (3) by setting $\mathbf{u} = [\omega r t + \delta u_\phi(r)]\hat{\phi}$, where ω is a constant angular velocity and δu_ϕ is the deviation from the mean displacement. Since the vortex lattice moves coherently over the whole system, we should impose the slip boundary condition $\sigma^{\mathrm{el}}_{r\phi} = 0$ at $r = R_1$ and R_2.[7] As a result, we obtain

$$\sigma^{\mathrm{el}}_{r\phi} = -\frac{B_0 I}{4\pi \ell}\left[1 - \frac{r^2}{R_1^2 + R_2^2} - \frac{R_1^2 R_2^2}{r^2(R_1^2 + R_2^2)}\right], \tag{5}$$

whose absolute value takes the maximum at $r = \sqrt{R_1 R_2}$. The angular velocity ω is given by

$$\omega = \frac{B_0 I}{\pi \ell\, \gamma (R_1^2 + R_2^2)}. \tag{6}$$

In the experiment,[3,4] above some critical current I_{cr} the shear stress becomes strong enough to break rigid rotations, result-

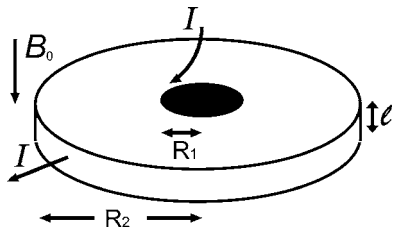

FIG. 1. Schematic illustration of the Corbino disk geometry. A magnetic field B_0 parallel to the disk axis is applied, and a current I is injected at the center of the disk and is ejected at the outer boundary. The radii of inner and outer rims are R_1 and R_2, respectively.

ing in the plastic motion of vortices. That is, the sample breaks into rings, with the inner portion rotating faster than the outer portion. Motivated by the experiment,[3,4] several researchers have investigated the plastic motion of vortex solids from theoretical[8–10] and numerical viewpoints.[11,12] However, because of the considerable difficulty from the first-principles approach, there is still no reliable nonlinear theory which can explain the general features of the complicated dynamics of vortex solids. Hence, we believe that a phenomenological approach is useful at the present stage.

II. PHENOMENOLOGICAL MODEL

Over the years, in many classes of physical systems with some crystalline orders, the nonlinear dynamical properties have been investigated by the Frenkel-Kontorova (FK) model or its extensions.[13] The basis of this approach is the following. First, we extract some relevant degrees of freedom from an original complicated nonlinear system (coarse graining or extracting a low-dimensional subsystem). Then, the dynamics is described by an effective periodic potential which is due to the eliminated degrees of freedom. In spite of the simplicity of the FK model, we can frequently deduce many important results for realistic physical problems.[13]

The slip (sliding) phenomena in various systems have been also studied by the FK model. Before proceeding further, let us mention several related examples. One of the most important applications of the FK model is the dislocation dynamics in metals. It is well known that a phenomenological FK-like model can provide a qualitative description of the slip process, which is the so-called Peierls-Nabarro model.[14,15] In the classical Peierls-Nabarro model, one regards a slip plane as a substrate. A dislocation moves, experiencing a periodic potential energy of displacement with a period related to the atomic spacing. In soft matter physics, previously Doi *et al.*[16] successfully explained an anomalous viscoelastic behavior observed in a hexagonal crystal phase of block copolymers within the framework of a one-dimensional (1D) FK model assuming the relative slippage of macrolattice layers.

In this paper, instead of considering from first principles, we introduce our simple phenomenological model based on the following idea reflecting the concept of the FK model.[17]

(i) In a rotating state the vortices are assumed to move on concentric circles to reduce excess drag. Moreover, we assume the vortices present local order, constructing a triangular lattice with the average lattice constant $\bar{a} \cong 2D/\sqrt{3}$, where D is the layer spacing. In the experimental condition,[4] $\bar{a} \sim 100$ Å, $R_1 \cong 35$ μm, and $R_2 \cong 350$ μm, so that the number of vortices in each layer is approximately 10^4–10^5. Here, as shown in Fig. 2, we notice that defects exist inevitably in order to adjust a triangular lattice into a Corbino disk geometry.

(ii) Above some critical current $I_{\rm cr}$ the shear stress becomes strong enough to break rigid rotations, resulting in the plastic motion of vortices. We now consider the elastic energy $E_{\rm el}$ of the shear deformation as follows. Let us suppose that the vortices of the $(n+1)$th and nth layers rotate by angles θ_{n+1} and θ_n on average, respectively. Note that, in this paper, θ_n is considered as a collective variable describing the nth-layer motion and the mean azimuthal displacement field of the nth layer is given by $u_n = nD\theta_n$. If the nth layer is regarded as a substrate of the $(n+1)$th layer, the vortices of the $(n+1)$th layer must climb over several potential barriers produced due to the vortices of the nth layer in the sliding state. The number of the potential barriers that each vortex climbs over is roughly estimated as $(\theta_{n+1}-\theta_n)/\Delta\theta_n$ on average, where $\Delta\theta_n \cong 2\pi/N_n \cong \bar{a}/nD$ is the average azimuthal angle interval of the adjacent vortices of the nth layer and N_n is the number of vortices contained in the nth layer. Similarly, the vortices of the nth layer must overcome approximately $(\theta_{n+1}-\theta_n)/\Delta\theta_{n+1}$ potential barriers in the sliding state. After the rotation, if the vortices construct a triangular lattice again, the energetically stable state is recovered. The situation stated here is outlined in Fig. 3. Thus, for the purpose of this paper, the coarse-graining shear elastic energy $E_{\rm el}$ is assumed to be given by the simple form

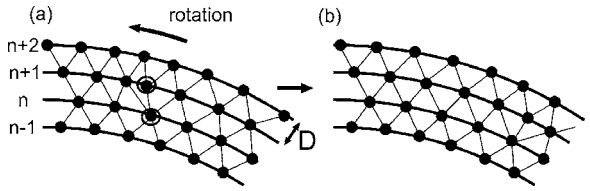

FIG. 2. Schematic figures of the rotating vortices, where we assume that they move on concentric circles, constructing a triangular lattice. In (a) we circle the fivefold and sevenfold neighboring vortices, which must exist in order to adjust a triangular lattice into a Corbino disk geometry. The vortices rotate from state (a) to (b). After the rotation, a likely equivalent state is realized, where the vortices construct a triangular lattice again.

$$E_{\rm el}\{\theta_n\} = \sum_{n=n_1+1}^{n_2-1} N_n \ell W \left[1 - \frac{1}{2}\cos\left(2\pi \frac{\theta_{n+1}-\theta_n}{\Delta\theta_{n+1}} \right) - \frac{1}{2}\cos\left(2\pi \frac{\theta_n - \theta_{n-1}}{\Delta\theta_{n-1}} \right) \right], \tag{7}$$

where ℓW is the strength of the potential barrier per vortex assumed to be a phenomenological parameter and the layers are numbered from n_1 to n_2.

(iii) The azimuthal elastic force $f_n^{\rm el}$ which acts on the nth layer is given by $-(\partial E_{\rm el}/\partial u_n) = -(\partial E_{\rm el}/\partial\theta_n)/nD$. From Eq. (7) we obtain

$$f_n^{\rm el} = \frac{2\pi^2 D\ell W}{\bar{a}^2} \left\{ (n+1)\left[\sin\left(\frac{\kappa_{n+1}}{\Delta\theta_{n+1}} \right) + \sin\left(\frac{\kappa_{n+1}}{\Delta\theta_n} \right) \right] - (n-1)\left[\sin\left(\frac{\kappa_n}{\Delta\theta_n} \right) + \sin\left(\frac{\kappa_n}{\Delta\theta_{n-1}} \right) \right] \right\}, \tag{8}$$

where $\kappa_n = 2\pi(\theta_n - \theta_{n-1})$. Therefore, the force balance equation for the nth layer is

$$0 = 2\pi nD^2 \ell \left(-\gamma \dot{u}_n + \frac{B_0 I}{2\pi\ell} \frac{1}{nD} \right) + f_n^{\rm el}, \tag{9}$$

where we make use of the condition that the number of vortices per unit area be approximately $1/(\bar{a}D)$. When the strain

rate is small enough, $n(\theta_{n+1}-\theta_n)\ll 1$, Eq. (9) can be reduced to the linearized equations (3) and (4) in the continuum limit $nD\to r$, with $W=c_{66}\bar{a}^2/2\sqrt{3}\pi^2$.

We have to notice that the above phenomenology is somewhat simplified. Complicated dislocation dynamics should be taken into account in order to explore detailed dynamic behaviors, such as shear-induced unbinding of dislocation pairs,[9] dynamics of grain boundaries,[11,12] etc. However, it is difficult to construct a satisfactory model in which the whole microscopic elementary processes are taken into account. Although our model is regarded as a mean-field-like model, it reproduces the major features of experimental results shown below.

III. NUMERICAL RESULTS

We will only present the numerical results obtained by solving Eq. (9). A detailed analysis and investigation will be presented elsewhere.[21] First of all, by measuring length and time in units of D and $\gamma D^2/c_{66}$, respectively, we rewrite Eq. (9) with Eq. (8) in the dimensionless form

$$0=-n\dot{\theta}_n+\frac{\lambda}{n}+\frac{n+1}{2\sqrt{3}\pi n}\{\sin[\sqrt{3}\pi(n+1)\kappa_{n+1}]+\sin(\sqrt{3}\pi n\kappa_{n+1})\}-\frac{n-1}{2\sqrt{3}\pi n}\{\sin(\sqrt{3}\pi n\kappa_n)+\sin[\sqrt{3}\pi(n-1)\kappa_n]\},\quad(10)$$

where $\lambda=B_0 l/2\pi\ell c_{66}$ is a dimensionless parameter characterizing the strength of the Lorentz force relative to the elastic force. In our numerical simulation we set $n_1=70$ and $n_2=700$. Furthermore, the slip (stress-free) boundary condition is used at $n=n_1$ and n_2.[22] In the linear regime, the absolute value of the shear stress takes the maximum of 0.401λ at $n=221\cong\sqrt{70\times 700}$ from Eq. (5) and the angular velocity is $4.04\lambda\times 10^{-6}$ from Eq. (6). We numerically solve Eq. (10) by the Runge-Kutta method.

In Fig. 4, the time-averaged angular velocity $\langle\omega_n\rangle=\langle\dot{\theta}_n\rangle$ is plotted, where $\langle\cdots\rangle$ denotes the time average and the average is taken over the period $\sim 10^6$ in the dynamical steady state. We can see that for low enough applied currents (in the linear regime) the vortices move coherently. However, above the critical value $\lambda_{cr}\cong 0.46$ the shear stress becomes strong enough to break rigid rotations, resulting in the plastic motion of vortices. That is, in the plastic regime the sample breaks into rings, with the inner portion rotating faster than the outer. The detailed behavior of $\langle\omega_n\rangle$ for several λ near λ_{cr} is shown in the inset of Fig. 4, where we can see that the plastic instability occurs near $n\cong 221$, as is expected from the linear analysis. Moreover, we notice that the interface between the faster band and slower band becomes wider as λ increases. This is because the region where the stress reaches the yield value expands with increasing the applied current. In the Appendix, we simply estimate the angular velocity, and the results for $\lambda=0.625$ and 0.875 are shown by the dotted lines in Fig. 4.

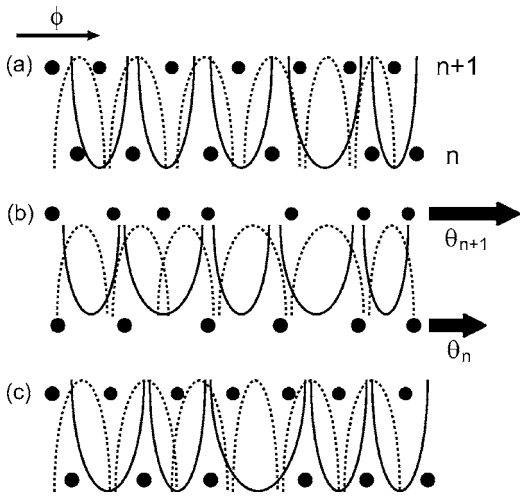

FIG. 3. Schematic figures of the relative slippage between the $(n+1)$th and nth layers, where the solid circles represent vortices and ϕ increases in the horizontal direction. The solid and dashed curves represent potential barriers due to the vortices of the nth and $(n+1)$th layers. (a) The system is assumed to be in an energetically stable configuration, where the vortices form a local order with a triangular lattice. In this state, though most potential minima trap only a single vortex, there always exist potential minima trapping two or more vortices and those trapping no vortex. This can be found from Fig. 2. (b) During the sliding motion, each vortex of both layers must overcome several potential barriers. (c) Another stable state is realized again.

In the experiment,[4] to spatially resolve the radial dependence of the angular velocity, the voltage differences were measured along a radius in the interval of 60 μm with $R_1=35$ μm and $R_2=350$ μm. The dimensionless form of the experimentally observed quantity is given by

$$\langle\omega_{i,i+1}\rangle=2\sum_{j=N_i+1}^{N_{i+1}}\frac{j\langle\omega_j\rangle}{(N_{i+1}-N_i)(N_{i+1}+N_i+1)},\quad(11)$$

where $N_i=70+120i$ $(i=1,2,3,4)$. If the vortex lattice rotates coherently, $\langle\omega_{1,2}\rangle=\langle\omega_{2,3}\rangle=\langle\omega_{3,4}\rangle$. In Fig. 5 we plot $\langle\omega_{i,i+1}\rangle$ as

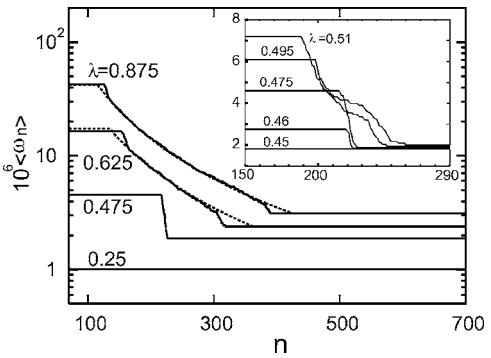

FIG. 4. The time-averaged angular velocities $\langle\omega_n\rangle$ for various values of λ. We can see that above the critical value λ_{cr} the shear stress becomes strong enough to break rigid rotations, resulting in the plastic motion of vortices. The dotted lines represent Eqs. (A2)–(A4) in the Appendix for $\lambda=0.625$ and 0.875. The inset shows more detailed behavior of $\langle\omega_n\rangle$ for several λ near λ_{cr}.

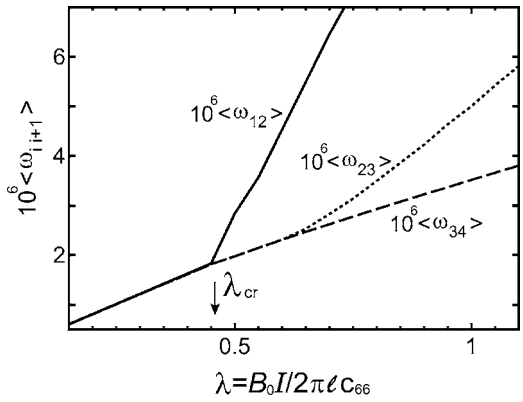

FIG. 5. $\langle\omega_{i,i+1}\rangle$ as functions of λ. For λ below λ_{cr}, $\langle\omega_{1,2}\rangle = \langle\omega_{2,3}\rangle = \langle\omega_{3,4}\rangle$; that is, the vortices rotate coherently. For λ above λ_{cr}, however, the rigid rotation breaks down.

functions of λ, which shows the shear-induced breakdown of rigid rotation above λ_{cr}. A similar plot can be seen in Fig. 4 of Ref. 4, and we find that the qualitative behavior of $\langle\omega_{i,i+1}\rangle$ is very consistent with the experimental results.

We evaluate the dimensionless parameter λ_{cr} from the experimental condition. In the experiment, $\ell \cong 10\ \mu$m, $B_0 \cong 5$ T, and the rigid rotation breaks down at $I \cong 10$ mA. Therefore, if we adopt a reasonable value of the shear elastic modulus $c_{66} \sim 10^3$ J/m^3,[23] the dimensionless parameter λ_{cr} can be estimated as $\lambda_{cr} \sim 1$, which is also consistent with that obtained from our phenomenological model.

It is worthwhile to note the following. (i) The experimental system has about 50 times as many vortex layers as our model system. Here, we assume that the average lattice constant is approximately 100 Å in the experimental system. (ii) The ratio of the outer radius to the inner radius R_2/R_1 is the same in both the experimental and our model systems. (iii) From Eq. (5), the yield stress $-\lambda_{cr}c_{66}(R_2/R_1-1)^2/2(R_2^2/R_1^2+1)$ depends only on the ratio R_2/R_1. On the other hand, from Eq. (6), it is found that the angular velocity at $\lambda=\lambda_{cr}$, $2\lambda_{cr}c_{66}/\gamma(R_1^2+R_2^2)$, has a system-size dependence. Therefore, if we make the experimentally observed quantities dimensionless in the same way as done in Sec. III, though the dimensionless value of the yield stress can be of the same order, the corresponding value of the angular velocity will be about 4×10^{-4} times the value obtained from our numerical analysis.[24]

IV. CONCLUDING REMARKS

In this paper we have phenomenologically investigated the nonlinear current-driven vortex dynamics in the Corbino disk geometry. Though our phenomenology has been constructed as a mean-field-like model, it can successfully reproduce the major features of the experimental results by Lopez *et al.*[4] However, it must be noticed that our model should be further improved in order to study the present problem in detail. We make several remarks as follows.

(i) As mentioned above, in real phenomena, the complicated dislocation dynamics should be important. Benetatos and Marchetti pointed out that the plastic instability is triggered by the shear-induced unbinding of dislocation pairs.[9] A recent molecular dynamics simulation[11,12] shows that the creation of dislocation pairs and their unbinding occur repeatedly at the onset of the plasticity. Furthermore, the simulation suggests that the resultant dynamics of grain boundaries plays a crucial role in plastic phenomena for relatively high applied currents. They have not been considered in the present analysis.

(ii) Analyzing the time-dependent Ginzburg-Landau equation numerically is also informative, because we can reveal elementary processes of vortex dynamics.

(iii) In vortex systems of type-II superconductors, an "entangled" state was predicted in a vortex liquid phase,[25] and then the liquid flows can be highly nonlocal.[26,27] In such an "entangled" state, some "viscoelastic instabilities" might be observed, which are ubiquitous in polymeric systems.[28]

These issues will be discussed in a future work.[21]

ACKNOWLEDGMENTS

A.F. thanks Dr. Jun-ichi Fukuda and Professor Thoru Okuzono for valuable discussions. Thanks are also due to Dr. Hiroto Adachi for introducing this problem. This study is financially supported in part by JSPS.

APPENDIX

In this appendix, we shall simply estimate the width of the sliding region and the angular velocity within the framework of the continuum approximation. According to the numerical results shown in Fig. 4, we can divide the disk space into the following three regions: region I ($R_1 \leqslant r \leqslant R_3$), region II ($R_4 \leqslant r \leqslant R_2$), and region III ($R_3 \leqslant r \leqslant R_4$). Though the vortex lattice moves coherently in both regions I and II, the relative slippage of vortex layers occurs in region III. Here we set R_3 and R_4 to be the inner and outer radii of the sliding region, respectively.

First, we consider the angular velocity in region III. We numerically verified that the time average of the shear stress in region III is almost constant. Therefore, we can rewrite Eq. (3) as

$$-\gamma r\omega_{\mathrm{III}} + \frac{2\sigma_{\mathrm{st}}}{r} + \frac{B_0 I}{2\pi\ell\, r} \cong 0, \tag{A1}$$

where σ_{st} is the constant value of the time-averaged shear stress $\langle\sigma_{r\phi}\rangle$ in the dynamical steady state. Equation (A1) gives

$$\omega_{\mathrm{III}} \cong \frac{2}{\gamma r^2}\left(\sigma_{\mathrm{st}} + \frac{B_0 I}{4\pi\ell}\right) \quad (R_3 \leqslant r \leqslant R_4). \tag{A2}$$

Next, we calculate the angular velocities in regions I and II. By a procedure similar to that used to obtain Eq. (6), the angular velocities of the rigid-body rotation in regions I and II are given by

$$\omega_{\mathrm{I}} = \frac{B_0 I}{\pi\ell\ \gamma(R_1^2+R_3^2)} + \frac{4R_3^2\sigma_{\mathrm{st}}}{\gamma(R_3^4-R_1^4)} \tag{A3}$$

and

$$\omega_{\mathrm{II}} = \frac{B_0 I}{\pi \ell\ \gamma(R_2^2 + R_4^2)} + \frac{4R_4^2 \sigma_{\mathrm{st}}}{\gamma(R_4^4 - R_2^4)}, \tag{A4}$$

respectively. Here we make use of the boundary conditions $\sigma_{r\phi}=0$ at $r=R_1$ and R_2 and $\sigma_{r\phi}=\sigma_{\mathrm{st}}$ at $r=R_3$ and R_4.

Equation (A2) must coincide with Eq. (A3) at $r=R_3$, resulting in

$$R_3 = R_1 \sqrt{\frac{1}{2\tilde{\sigma}_{\mathrm{st}} + \lambda}[\lambda + \sqrt{\lambda^2 - (2\tilde{\sigma}_{\mathrm{st}} + \lambda)^2}]}, \tag{A5}$$

where $\tilde{\sigma}_{\mathrm{st}}=\sigma_{\mathrm{st}}/c_{66}$ and $\lambda=B_0 I/2\pi\ell c_{66}$. Similarly, R_4 is given by

$$R_4 = R_2 \sqrt{\frac{1}{2\tilde{\sigma}_{\mathrm{st}} + \lambda}[\lambda - \sqrt{\lambda^2 - (2\tilde{\sigma}_{\mathrm{st}} + \lambda)^2}]}. \tag{A6}$$

Equations (A5) and (A6) give the width of sliding region R_4-R_3.

In our numerical analysis, $|\tilde{\sigma}_{\mathrm{st}}| \cong 0.155$ for large λ, which is smaller than the absolute value of the yield stress ($\cong 0.184$). In Fig. 4, we plot Eqs. (A2)–(A4) with Eqs. (A5) and (A6) for $\lambda = 0.625$ and 0.875 by dotted lines. They are very consistent with the numerical results. Note that, however, there are deviations between the present simple estimation and the numerical results near λ_{cr}, where region III is so narrow that Eq. (A2) does not hold well.

[1] G. W. Crabtree and D. R. Nelson, Phys. Today **50** (4), 38 (1997).

[2] G. Blatter, M. V. Feigel'man, V. B. Geshkenbein, A. I. Larkin, and V. M. Vinokur, Rev. Mod. Phys. **66**, 1125 (1994).

[3] G. W. Crabtree, Nat. Mater. **2**, 435 (2003).

[4] D. Lopez, W. K. Kwok, H. Safar, R. J. Olsson, A. M. Petrean, L. Paulius, and G. W. Crabtree, Phys. Rev. Lett. **82**, 1277 (1999); G. W. Crabtree, D. Lopez, W. K. Kwok, H. Safar, and L. M. Paulius, J. Low Temp. Phys. **117**, 1313 (1999).

[5] T. Nattermann and S. Scheidl, Adv. Phys. **49**, 607 (2000).

[6] J. Bardeen and M. J. Stephen, Phys. Rev. **140**, 1197A (1965).

[7] In Ref. 9, the slip (stress-free) boundary condition is given by $\nabla_r u_\phi = 0$. However, in cylindrical geometry, we must set $\nabla_r(u_\phi/r)=0$, because the shear stress in the linear elasticity is given by $c_{66} r \nabla_r(u_\phi/r)$. Therefore, Eqs. (5) and (6) are different from those in Ref. 9 which are obtained under a different boundary condition.

[8] M. C. Marchetti, Physica C **341**, 991 (2000).

[9] P. Benetatos and M. C. Marchetti, Phys. Rev. B **65**, 134517 (2002).

[10] A. A. Babaei Brojeny and J. R. Clem, Phys. Rev. B **64**, 184507 (2001).

[11] M.-C. Miguel and S. Zapperi, Nat. Mater. **2**, 477 (2003).

[12] M.-C. Miguel, P. Moretti, M. Zaiser, and S. Zapperi, Mater. Sci. Eng., A **400**, 191 (2005).

[13] O. M. Braun and Y. S. Kivshar, *The Frenkel-Kontorova Model: Concepts, Methods, and Applications* (Springer-Verlag, Berlin, 2004).

[14] R. Peierls, Proc. Phys. Soc. London **52**, 34 (1940).

[15] F. R. N. Nabarro, Proc. Phys. Soc. London **59**, 256 (1947).

[16] M. Doi, J. L. Hardeen, and T. Ohta, Macromolecules **26**, 4935 (1993).

[17] Several problems of vortex lattice dynamics have been also studied within the framework of the FK model (Refs. 18–20). In these studies the 1D motion of the vortex array on the stationary periodic substrate is mainly considered. In this paper, however, we consider the relative slippage of vortex layers. Thus, our approach is similar to that of Ref. 16 rather than those of Refs. 14, 15, and 18–20.

[18] R. Besseling, R. Niggebrugge, and P. H. Kes, Phys. Rev. Lett. **82**, 3144 (1999); R. Besseling, P. H. Kes, T. Dröse, and V. M. Vinokur, New J. Phys. **7**, 71 (2005), and references therein.

[19] C. Reichhardt and F. Nori, Phys. Rev. Lett. **82**, 414 (1999).

[20] M. C. Marchetti, A. A. Middleton, and T. Prellberg, Phys. Rev. Lett. **85**, 1104 (2000).

[21] A. Furukawa (unpublished).

[22] The force which acts from the $(n+1)$th layer to the nth layer is proportional to $\{\sin[2\pi(\theta_{n+1}-\theta_n)/\Delta\theta_{n+1}]+\sin[2\pi(\theta_{n+1}-\theta_n)/\Delta\theta_n]\}$. Hence, the slip (stress-free) boundary conditions for the present discrete layers are given by $\theta_{n_2}=\theta_{n_2-1}$ and $\theta_{n_1+1}=\theta_{n_1}$. They are consistent with those for the linear elasticity, $\nabla_r(u_\phi/r)=0$, in the continuum limit.

[23] E. H. Brandt, Rep. Prog. Phys. **58**, 1465 (1995); K. Fossheim and A. Sudbø, *Superconductivity: Physics and Applications* (Wiley, London, 2004). In our estimation, we assume that the penetration length is of the order of several hundreds of nm.

[24] The unit time is estimated as $\gamma D^2/c_{66}=\sqrt{3}\Phi_0 B_{c2}/2\rho_{\mathrm{n}} c_{66} \sim 10^{-10}$ s, where $\Phi_0=h/2e=2.07\times10^{-15}$ W b is the magnetic flux quantum, $B_{c2}\sim 100$ T is the upper critical field, and $\rho_{\mathrm{n}} \sim 10^{-6}\ \Omega$ m is the normal-state resistivity (Refs. 2 and 23). Thus, the angular velocity at λ_{cr} of our model system corresponds to about 10^4 s^{-1}. If our model system has the same number of layers as the experimental system, the angular velocity is of the same order as that observed in the experiment (Ref. 4).

[25] D. R. Nelson, Phys. Rev. Lett. **60**, 1973 (1988).

[26] M. C. Marchetti and D. R. Nelson, Phys. Rev. B **42**, 9938 (1990); Physica C **174**, 40 (1991).

[27] D. A. Huse and S. N. Majumdar, Phys. Rev. Lett. **71**, 2473 (1993).

[28] R. G. Larson, *The Structure and Rheology of Complex Fluids* (Oxford University Press, Oxford, 1999).